SUPPORTING INFORMATION

Synthesis of supported planar iron oxide nanoparticles and their chemo– and stereoselectivity for hydrogenation of alkynes.

María Tejeda–Serrano,[a] Jose R. Cabrero–Antonino,[a,b] Virginia Mainar–Ruiz,[a] Miguel López–Haro,[c] Juan C. Hernández–Garrido,[c] José J. Calvino,[c] Antonio Leyva–Pérez,[a*] and Avelino Corma.[a*]

[a] Instituto de Tecnología Química. Universidad Politècnica de València–Consejo Superior de Investigaciones Científicas. Avda. de los Naranjos s/n, 46022, Valencia, Spain.
[b] Leibniz-Institut fir Katalyse e.V., Albert-Einstein-Str. 29a, 18059 Rostock (Germany).
[c] Departamento de Ciencia de Materiales e Ingeniería Metalúrgica y Química Inorgánica, Universidad de Cádiz, Campus Río San Pedro, Puerto Real, 11510 Cádiz, Spain.

Corresponding authors: acorma@itq.upv.es, anleyva@itq.upv.es.

Table of Contents:

General.

Reagents and solvents were obtained from commercial sources (Aldrich) and were used without further purification otherwise indicated. All the products obtained were characterised by GC-MS, ^{1}H- and ^{13}C-NMR, and DEPT. When available, the characterisation given in the literature was used for comparison. Gas chromatographic analyses were performed in an instrument equipped with a 25 m capillary column of 5% phenylmethylsilicone. GC/MS analyses were performed on a spectrometer equipped with the same column as the GC and operated under the same conditions. ^{1}H, ^{13}C and DEPT were recorded in a 300 MHz instrument using $CDCl_3$ as solvent containing TMS as an internal standard. Elemental analyses of the solids and some products were determined by chemical combustion using a CHNSO analyzer. Absorption spectra were recorded on an UV/Vis spectrophotometer (UV0811M209, Varian).

High Resolution Electron Microscopy (HREM) experiments were performed in a JEOL2010F microscope operating at 200 kV. The structural resolution characteristic of this microscope, equipped with a narrow gap pole piece is 0.19 nm. Images were digitally recorded on a Gatan 2k x 2k CCD camera. HREM images were analyzed in the Fourier domain using Digital Micrograph Microscopy suite routines. The analytical studies by X-EDS spectroscopy were performed in a TEM-STEM aberration corrected FEI Titan3 Themis 60-300 microscope operating at 80 kV. A condenser aperture of 50 μm and a 91 mm camera length was used, obtaining an electron probe with a convergence angle of 20 mrad. In order to get a high signal-to-noise ratio a beam current of 0.2 nA was used. The X-EDS hypermaps were recorded using a Super-X EDS detector, a 4 window-less X-EDS detectors surrounding the TEM sample. The background correction and the deconvolution to extract the contribution of the K lines of O, Ti and Fe were carried out using the Bruker proprietary software (Esprit 1.94). Quantification of the recorded hypermaps and spectra was performed using the theoretical zeta-factors for the K lines of Ti, Fe and O at 80 kV. In particular, Bote-Salvat Ionization Cross Sections and Hubble ionization yield were considered. STEM samples were prepared by depositing small amounts of the powder catalysts onto holey-carbon coated Cu grids. No solvent was used during this preparation to avoid contamination problems during STEM investigation. After preparation, samples were maintained under vacuum conditions at room temperature.

Figures.

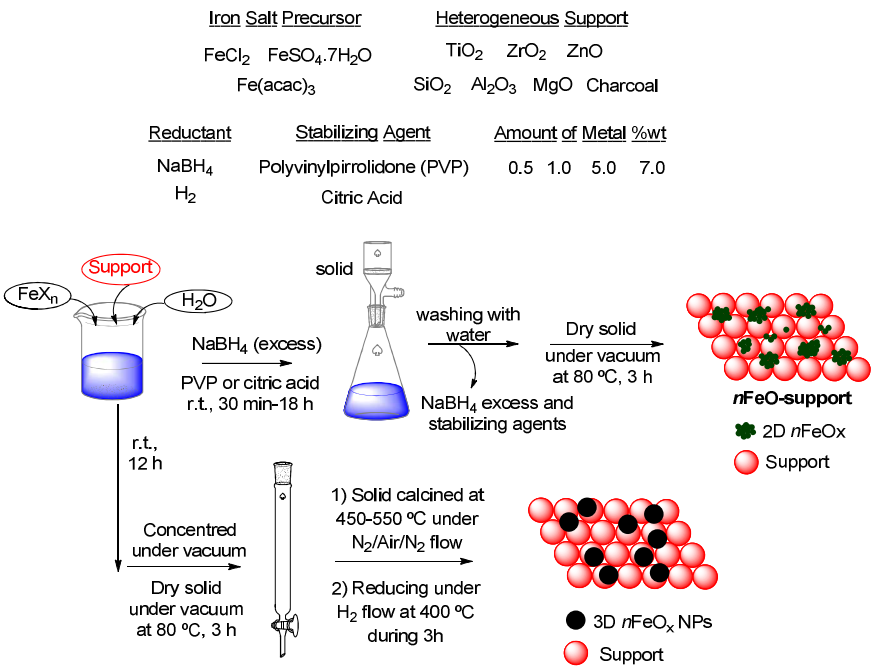

Figure S1. Complete set of conditions for the different FeOx supported materials synthesized and employed in this work. Blank experiments without organic stabilizer do not give similar materials neither in terms of characterization nor catalysis. It seems that the organic stabilizer is not innocent and could be involved in the formation of the planar FeO structures.

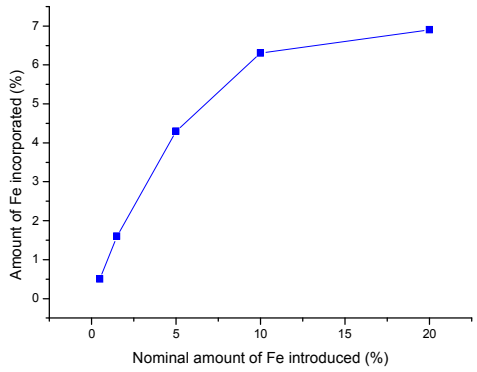

Figure S2. Amount of Fe incorporated into TiO_2 by inductively coupled plasma-mass spectroscopy (ICP-MS) as a function of the nominal amount introduced during the synthesis.

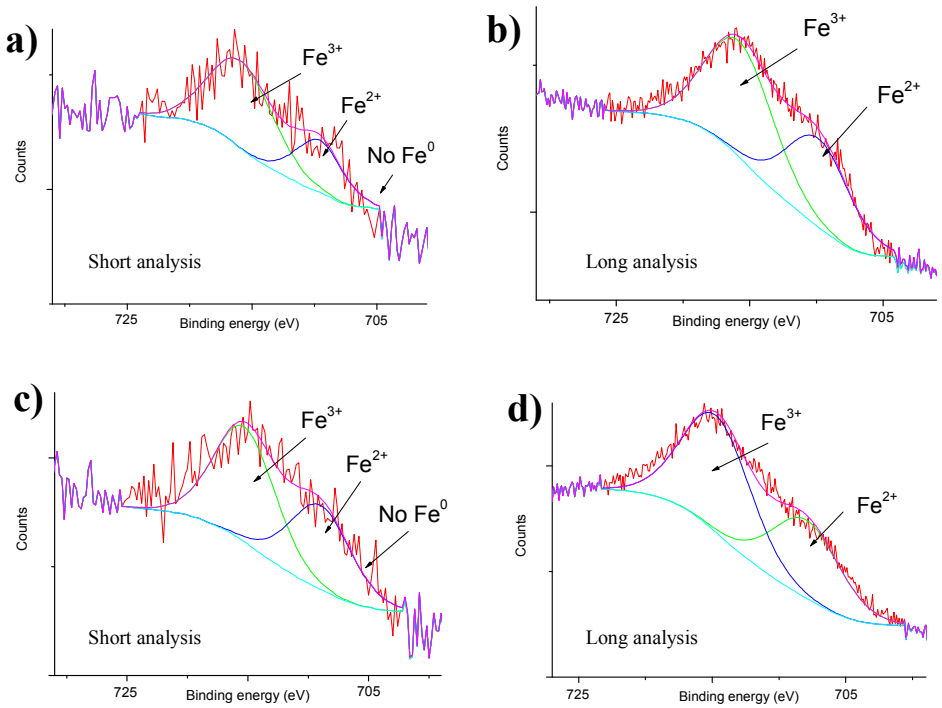

Figure S3. Deconvoluted $Fe_{2p3/2}$ XPS spectrum for two diffferent batches (top and bottom) of 5.0 wt% FeOx-TiO_2, recorded rapidly at the beginning of the spectroscopic study to avoid reduction by the XPS beam (a and c) or recorded for long times (b and d).

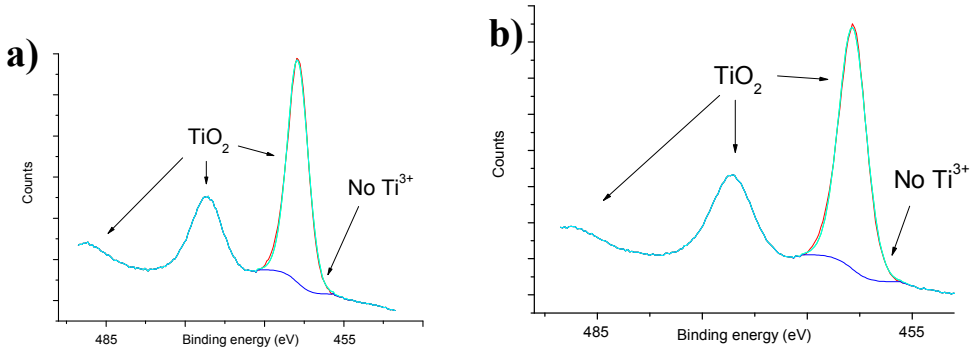

Figure S4. Deconvoluted $Ti_{2p1/2}$ XPS spectrum for 5 wt% FeOx-TiO_2 recorded at short (a) or at longer times (b).

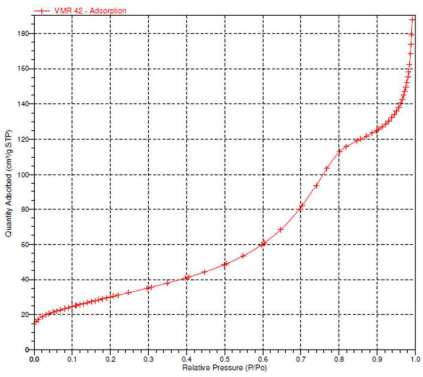

Figure S5. Representative N_2 adsorption-desorption isotherm for *n*FeOx supported on TiO_2. The Brunauer–Emmett–Teller (BET) surface value of the material, S_{BET}, is 111.38 m^2xg^{-1}, nearly identical to the original TiO_2 material (110 m^2xg^{-1}).

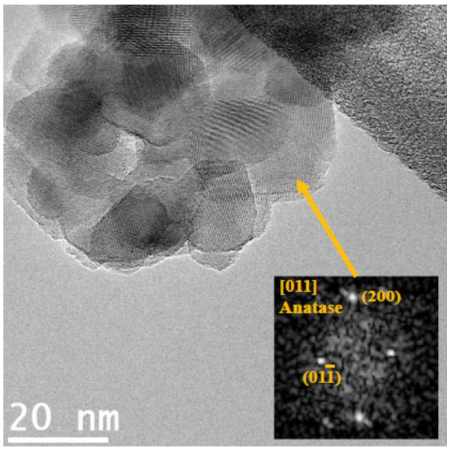

Figure S6. Representative HR-TEM image of the *n*FeO-TiO2 catalysts in bright-field mode. The digital diffraction pattern (DDP) of one of the crystallites (pointed by arrow) is shown as an inset.

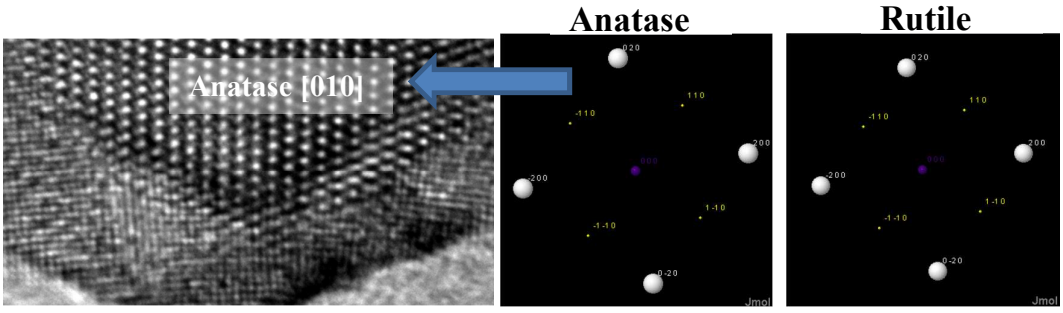

Figure S7. Representative HR-TEM image of *n*FeO-TiO_2 catalysts, in bright-field mode, where the presence of pure anatase phase is observed for TiO_2.

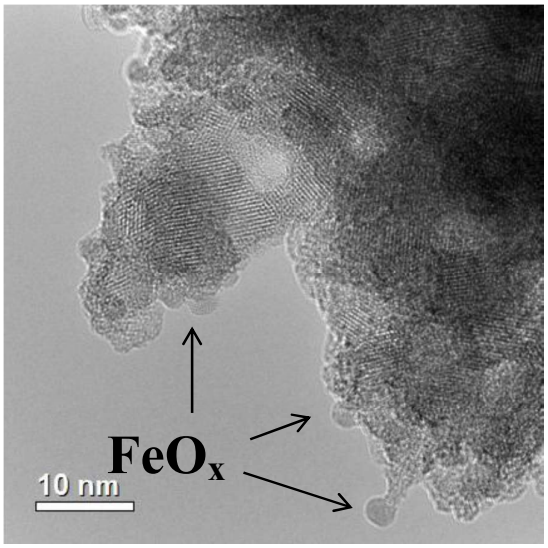

Figure S8. Representative micrograph high resolution aberration corrected transmission electron microscopy (HR-TEM) of 7.0 wt% *n*FeOx-TiO_2, in bright-field mode.

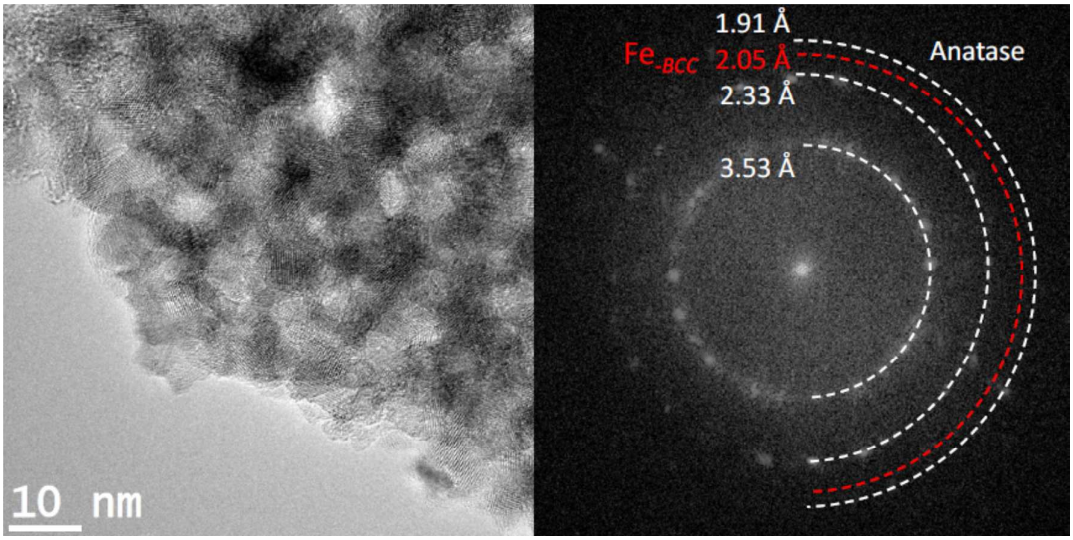

Figure S9. Representative HR-TEM image of the 0.5 or 1.0 wt% *n*FeO-TiO_2 catalysts, in bright-field mode. The DDP of the whole area is also shown, where the position of the diffraction rings corresponding to anatase and Fe-bcc are marked in white and red dashed lines, respectively. Note the absence of spots on the Fe-bcc ring.

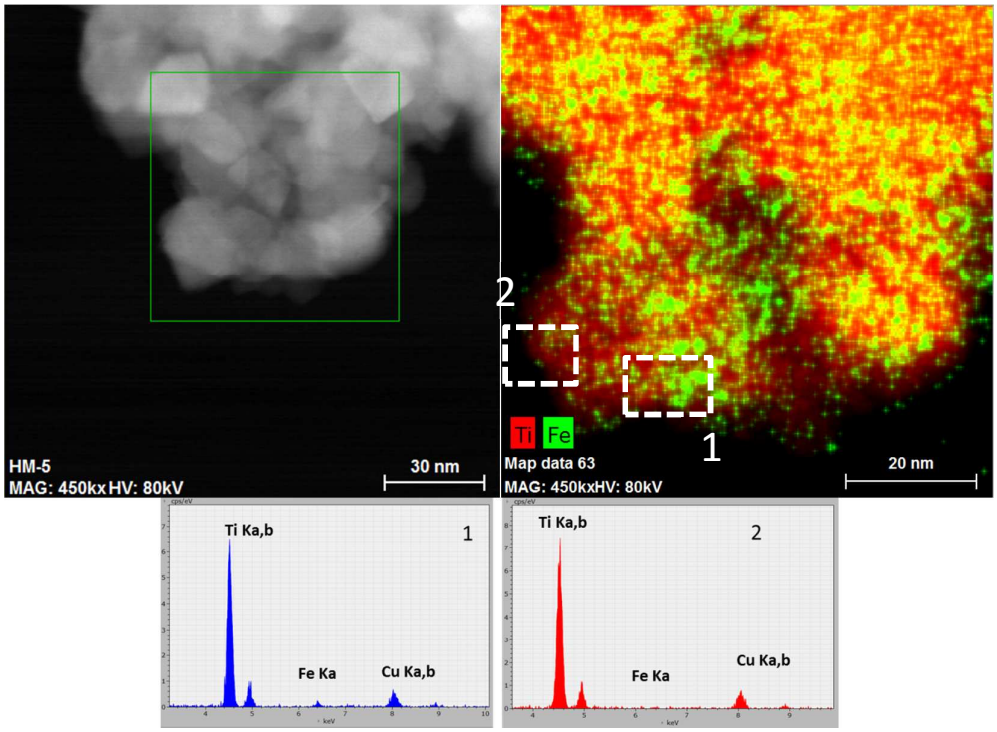

Figure S10. HAADF-STEM image of the 0.5 wt% *n*FeO-TiO_2 catalysts with the corresponding X-EDS mapping of the selected area for Fe (green) and Ti (red) atoms, and the elemental analysis of the squared areas.

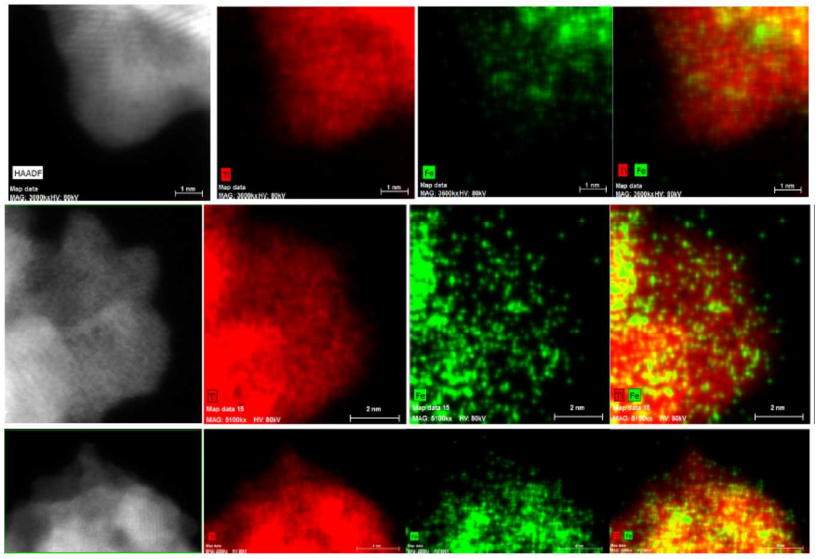

Figure S11. X-EDS elemental maps recorded on different locations of the 0.5 wt% *n*FeO-TiO_2 catalyst. The left column shows the HAADF-STEM images corresponding to each location. Middle columns correspond to the Ti and Fe distribution maps (labeled). A composite Fe/Ti map is shown at the right column.

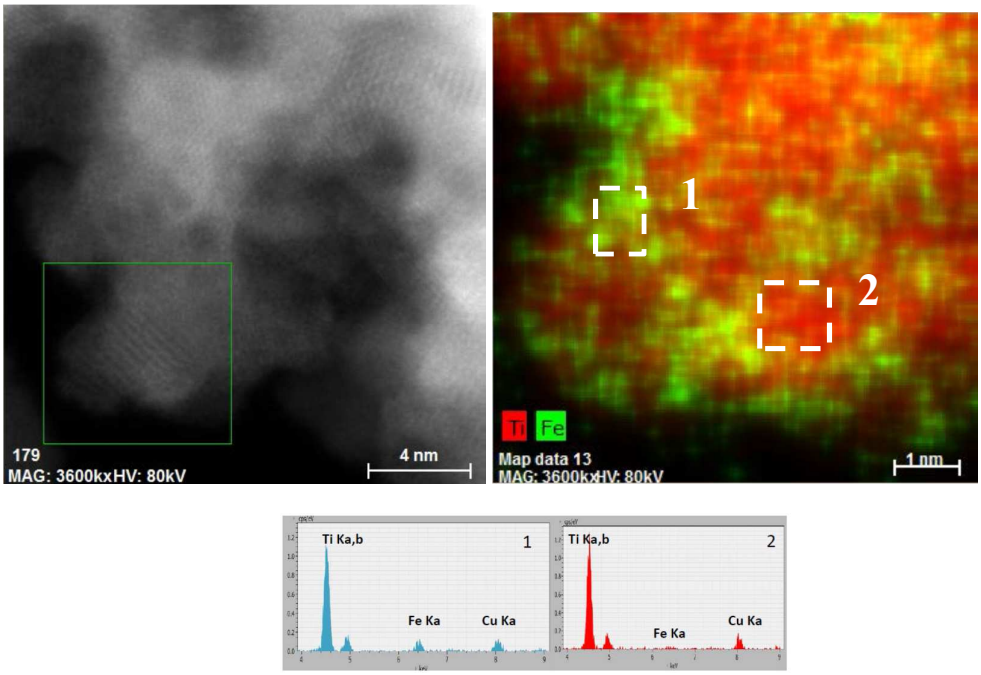

Figure S12. HAADF-STEM image of the 1.0 wt% *n*FeO-TiO_2 catalysts with the corresponding X-EDS mapping of the selected area for Fe (green) and Ti (red) atoms, and the elemental analysis of the squared areas.

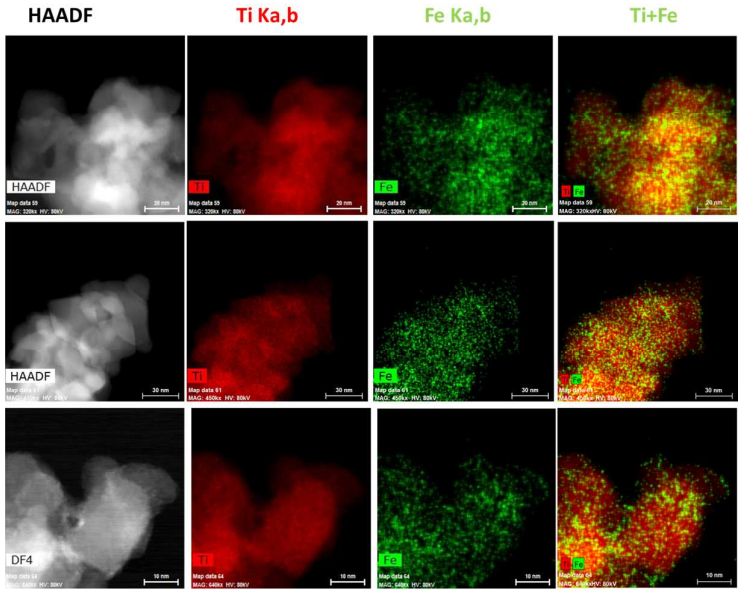

Figure S13. X-EDS elemental maps recorded on different locations of the 1.0 wt% *n*FeO-TiO_2 catalysts. The left column shows the HAADF-STEM images corresponding to each location. Middle columns correspond to the Ti and Fe distribution maps (labeled). A composite Fe/Ti map is shown at the right column.

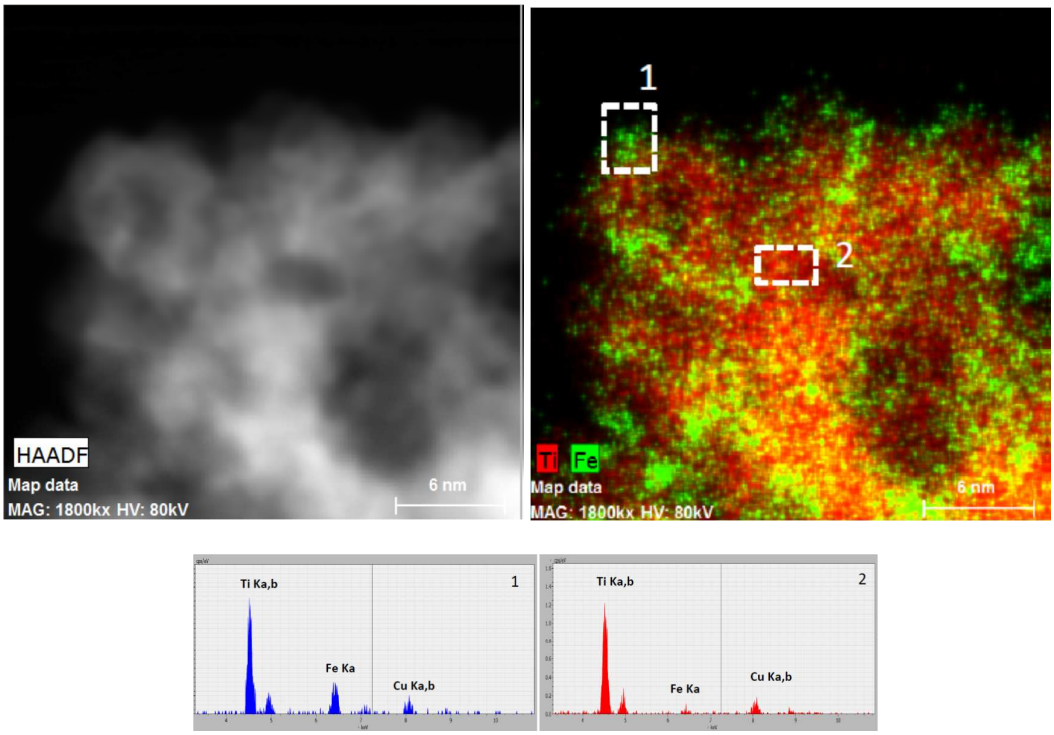

Figure S14. HAADF-STEM image of the 7.0 wt% *n*FeO-TiO_2 catalysts with the corresponding X-EDS mapping of the selected area for Fe (green) and Ti (red) atoms, and the elemental analysis of the squared areas.

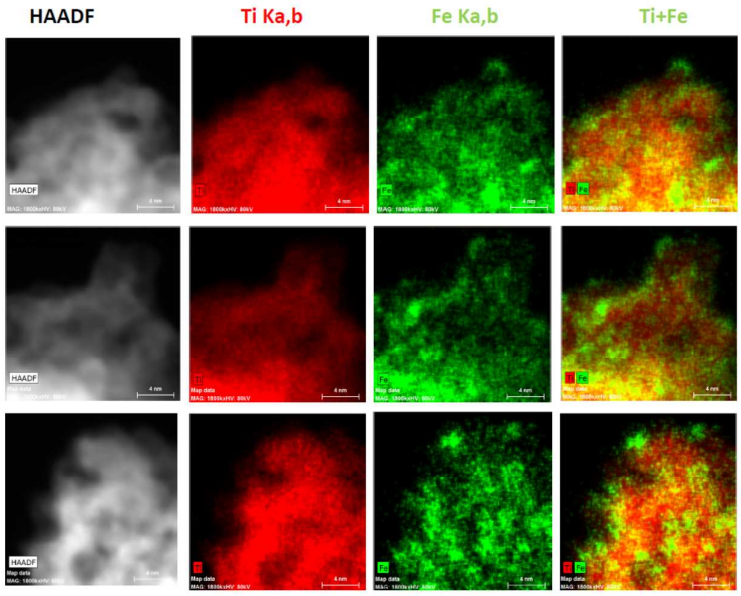

Figure S15. X-EDS elemental maps recorded on different locations of the 7.0 wt% *n*FeO-TiO_2 catalysts. The left column shows the HAADF-STEM images corresponding to each location. Middle columns correspond to the Ti and Fe distribution maps (labeled). A composite Fe/Ti map is shown at the right column.

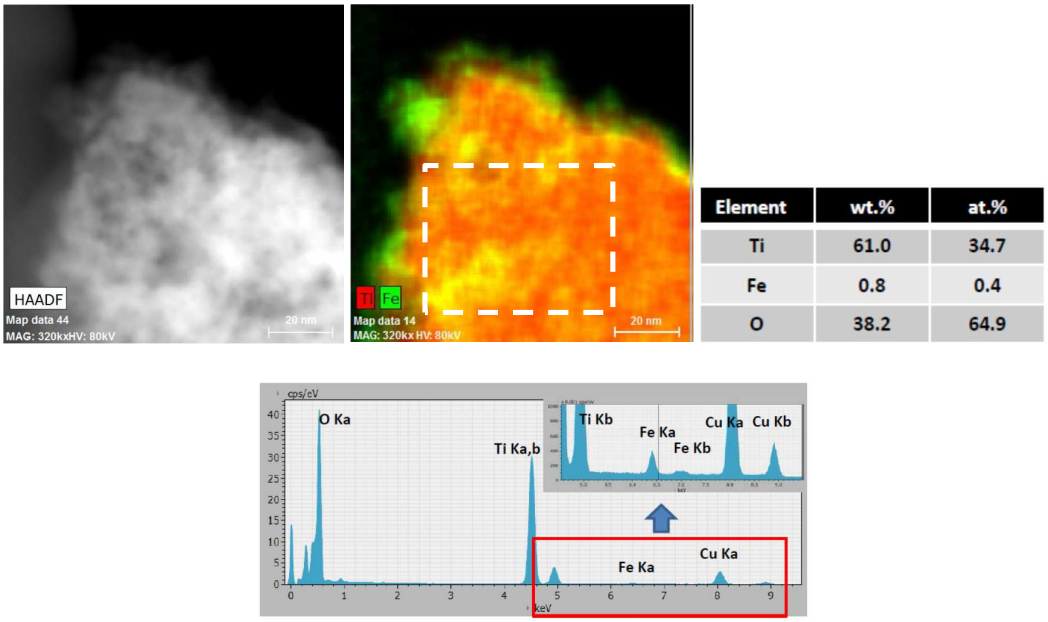

Element	wt.%	at.%
Ti	61.0	34.7
Fe	0.8	0.4
O	38.2	64.9

Figure S16. HAADF-STEM image of the 1.0 wt% *n*FeO-TiO_2 catalysts with the corresponding deconvoluted X-EDS mapping of the selected area for Fe (green) and Ti (red) atoms, and the elemental analysis of the square area with the obtained Cliff-Lorimer quantification.

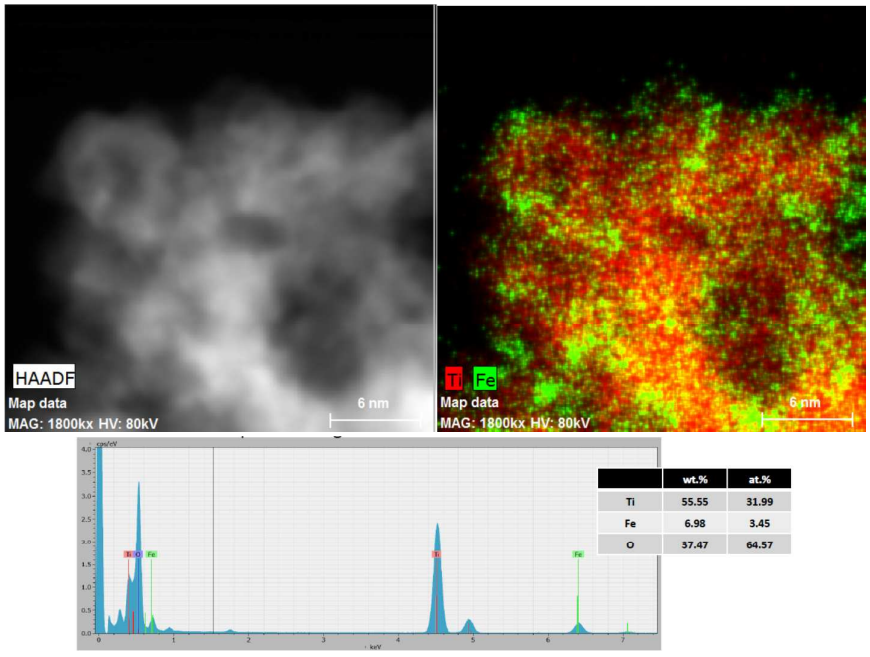

	wt.%	at.%
Ti	55.55	31.99
Fe	6.98	3.45
O	37.47	64.57

Figure S17. HAADF-STEM image of the 7.0 wt% *n*FeO-TiO_2 catalysts with the corresponding deconvoluted X-EDS mapping for Fe (green) and Ti (red) atoms, and the elemental analysis with the obtained Cliff-Lorimer quantification.

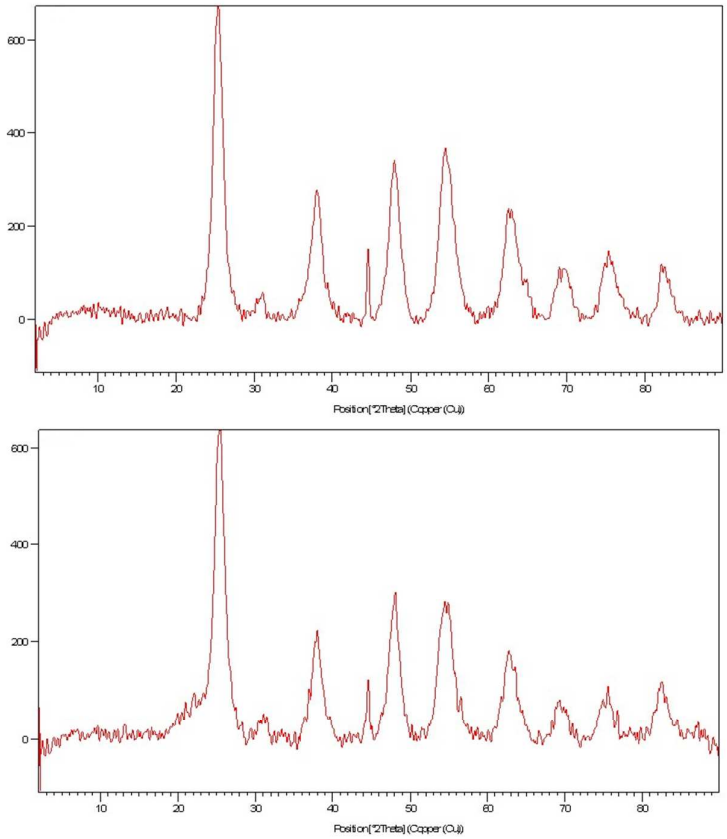

Figure S18. X-ray diffraction (XRD) of different 2D *n*FeOx-TiO_2 solids. Top: 0.5 wt% Fe by one-pot synthesis. Bottom: 7 wt% Fe by the two-step synthesis.

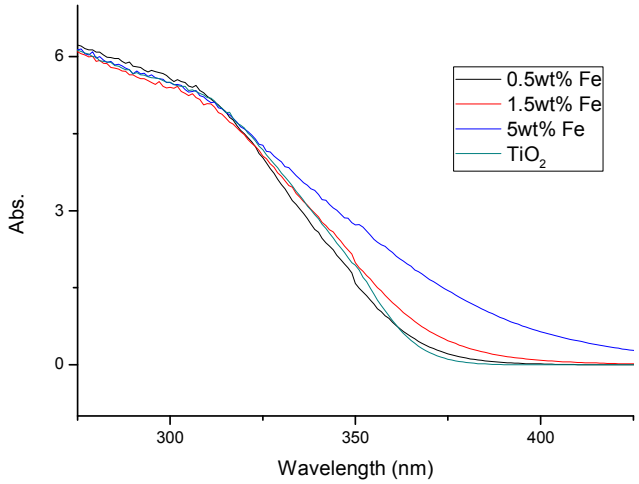

Figure S19. Reflectance-diffuse ultraviolet-visible spectroscopy (RDUV-vis) of different *n*FeOx-TiO_2 solids.

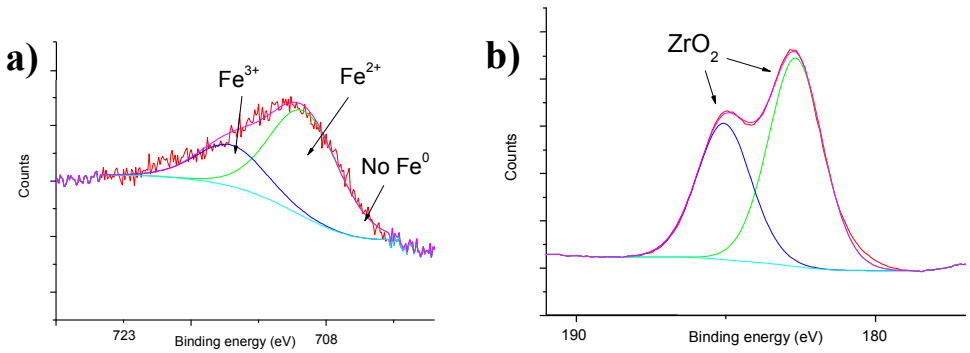

Figure S20. Deconvoluted $Fe_{2p3/2}$ (a) and $Zr_{3d5/2}$ (b) XPS spectra for 5 wt% ZrOx-TiO_2.

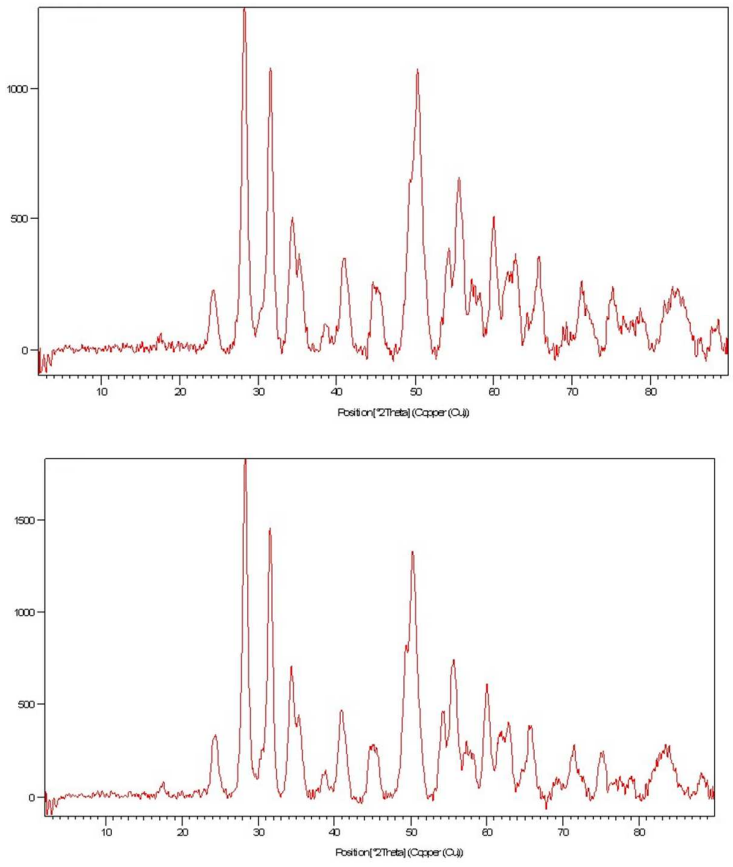

Figure S21. X-ray diffraction (XRD) of different *n*FeOx-ZrO_2 solids. Top: 1 wt% Fe by one-pot synthesis. Bottom: 3.8 wt% Fe by one-pot synthesis.

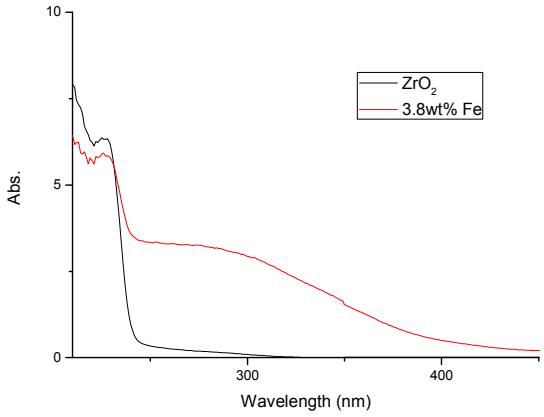

Figure S22. Reflectance-diffuse ultraviolet-visible spectroscopy (RDUV-vis) of different *n*FeOx-ZrO_2 solids.

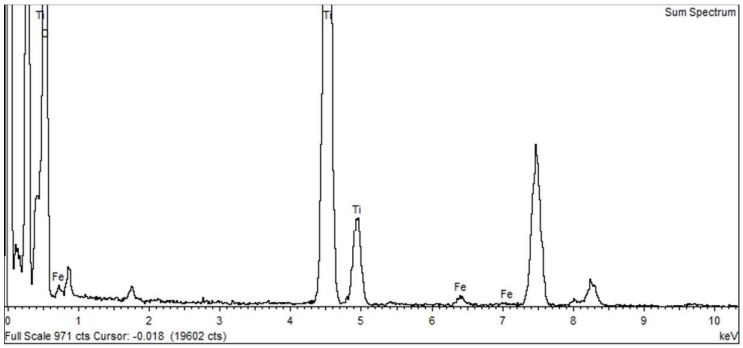

Figure S23. X-ray diffraction (XRD) of *n*FeOx supported on TiO_2 by the impregnation/calcination procedure. Diffracting 3D FeOx particles can be clearly seen.

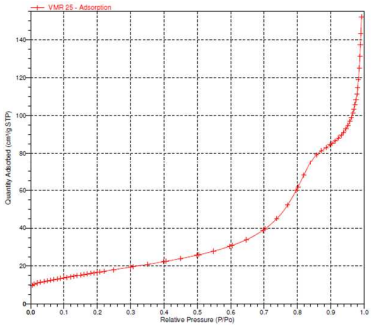

Figure S24. N_2 adsorption-desorption isotherms for *n*FeOx supported on TiO_2 with calcination, that according to the Brunauer–Emmett–Teller (BET) model gives a S_{BET} of 61.47 m^2xg^{-1}.

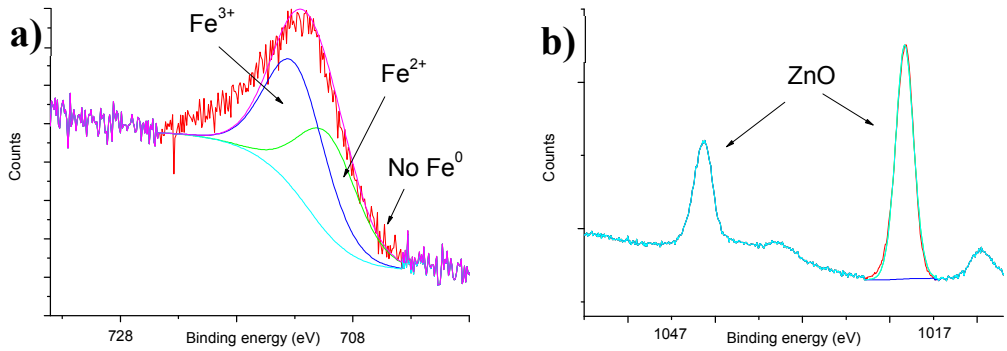

Figure S25. Deconvoluted $Fe_{2p3/2}$ (a) and $Zn_{2p3/2}$ (b) spectra for a sample of 5 wt% *n*FeOx-ZnO.

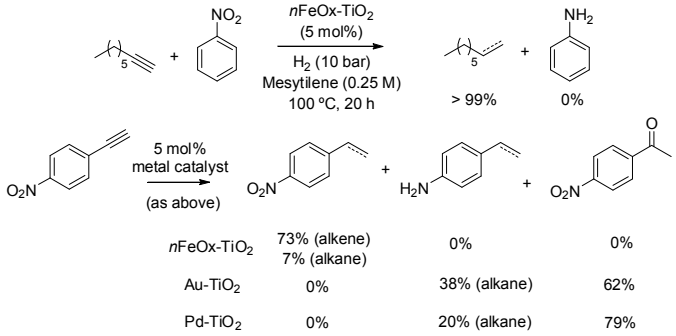

Figure S26. Comparison of *n*FeOx-TiO_2 with well-known Pd and Au hydrogenating catalysts supported on TiO_2, under the optimized reaction conditions for the former.

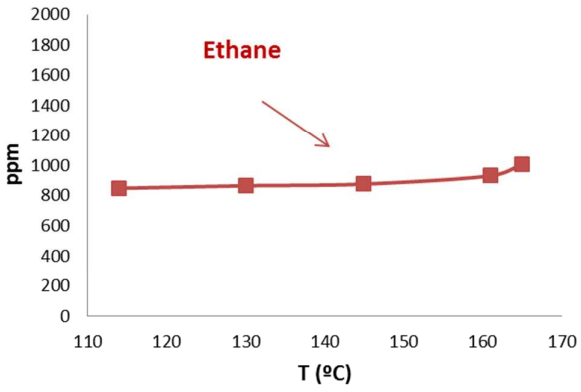

Figure S27. Ethane generated in a range of temperatures for the removal of 1% (10 000 ppm) of acetylene in a stream of ethylene with the *n*FeOx-TiO_2 catalyst (7.0 wt%). Reaction conditions: 4 equivalents of H_2 respect to ethylene, 1 ml·min^{-1} flow, 3 bar of pressure, 15 min reaction time for each temperature.

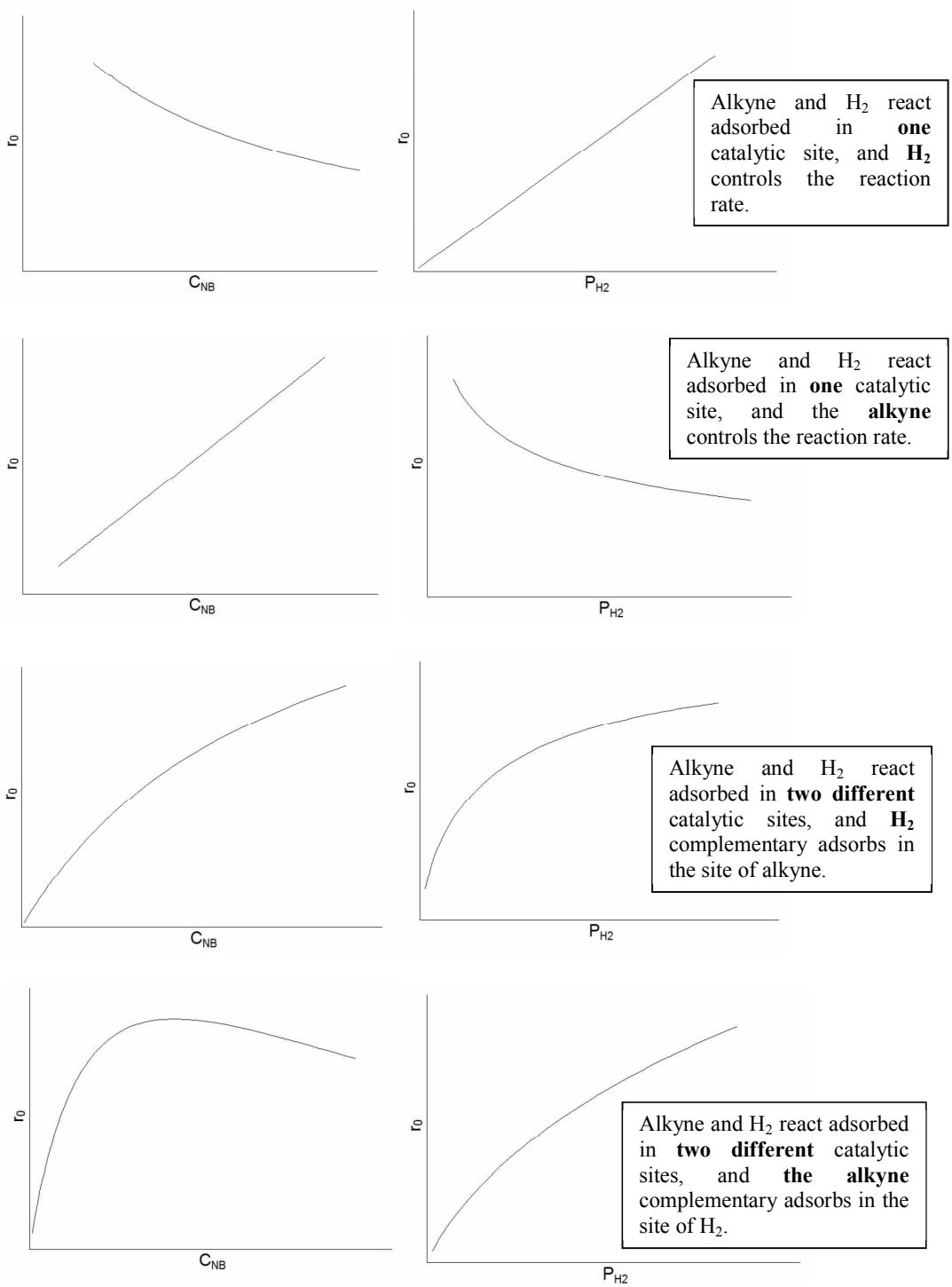

Figure S28. Four potential Langmuir-Hinshelwood/Hougen-Watson (LHHW) models for the kinetic results of the hydrogenation of 1-dodecyne **1a** catalyzed by *n*FeOx-TiO_2 (7.0 wt% Fe). Squared the best-fitted model.

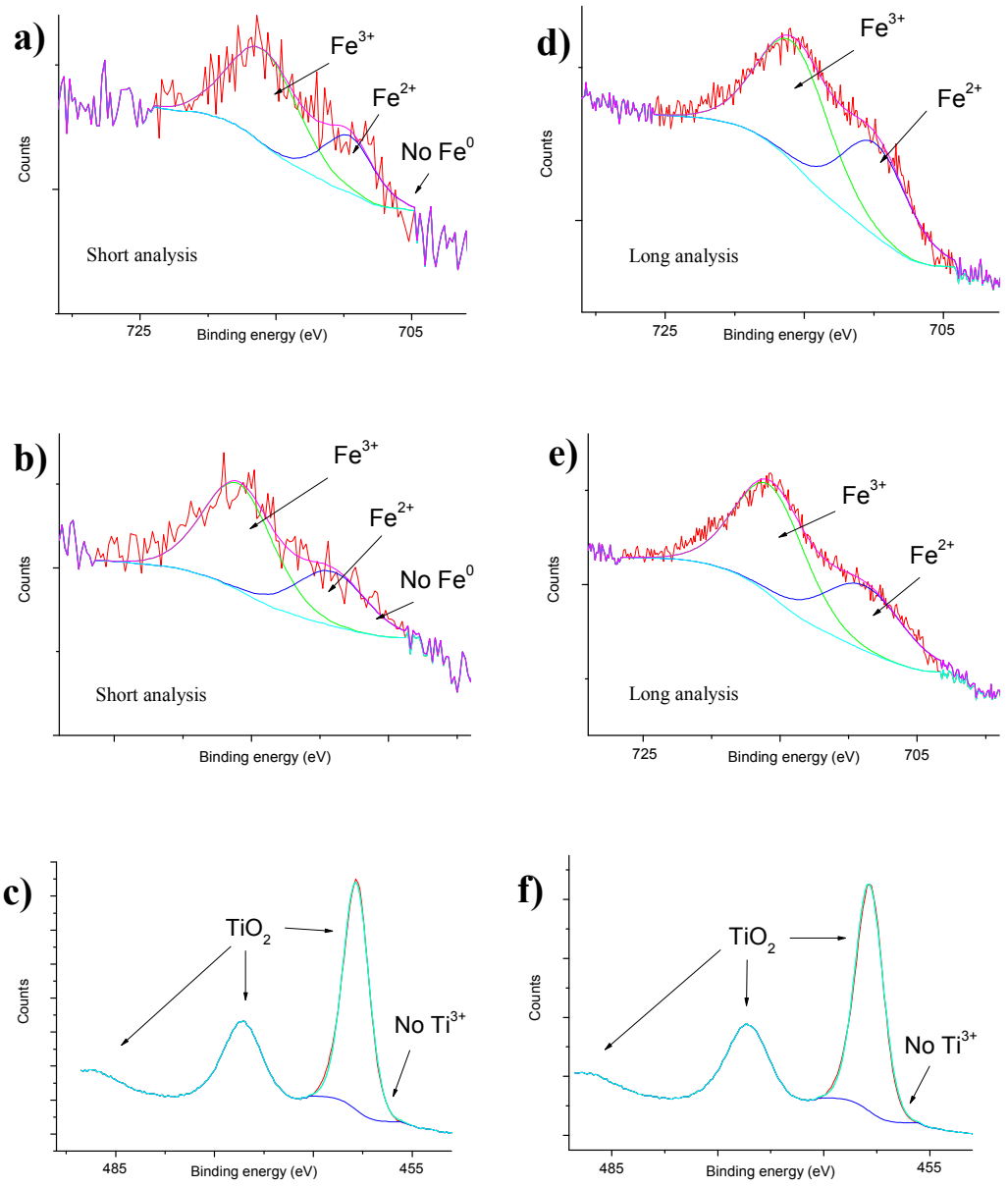

Figure S29. Evolution of the $Fe_{2p3/2}$ XPS spectrum of a 5 wt% FeOx-TiO_2 sample (top) treated under H_2 at 150 ºC in the XPS chamber (middle), recorded rapidly at the beginning of the measurement to avoid reduction by the XPS beam (a-c) or recorded for long times (d-f), and the same spectroscopic study for $Ti_{2p1/2}$ (bottom).

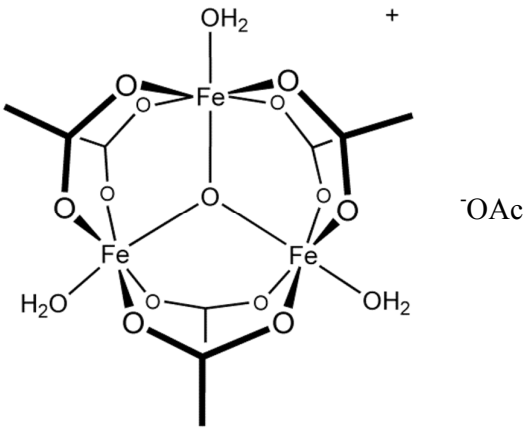

Figure S30. Structure of $[Fe_3(\mu_3\text{-}O)(OAc)_6(H_2O)_3]OAc$.

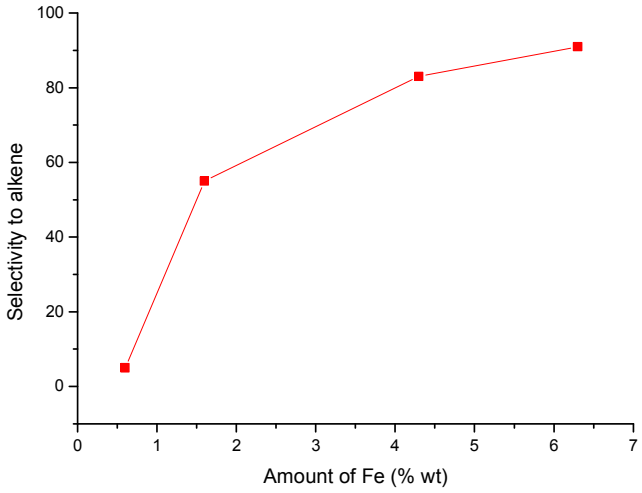

Figure S31. Selectivity for the hydrogenation of 1-dodecyne **1a** with different *n*FeOx-TiO_2 materials.

Table S1. ICP-MS results of the different Fe-supported solids.

Support	Reducing agent	Organic stabilizer	Fe salt precursor	% wt Fe (nominal)	% wt Fe found
TiO_2	$NaBH_4$ (two-step)	Citric acid	$FeCl_2$	1.5	1.624
				5	4.296
				10	6.286
				20	6.936
	$NaBH_4$ (one-step)	Citric acid	$FeCl_2$	0.5	0.504
			$FeSO_4 \cdot 7H_2O$		0.584
		PVP			0.501
			$FeCl_2$		0.641
		Citric acid		1.5	1.564
					1.564
	H_2	-	$FeCl_2$	0.5	0.608
			$FeSO_4 \cdot 7H_2O$	0.5	0.693
				1.5	1.949
			$FeCl_2$	1.5	1.870
ZrO_2	$NaBH_4$ (two-step)	Citric acid		0.5	0.561
				5	3.842
	$NaBH_4$ (one-step)			0.5	0.512
			$FeSO_4 \cdot 7H_2O$		0.535
			$Fe(acac)_3$		0.603
	H_2	-	$FeCl_2$		0.578
			$FeSO_4 \cdot 7H_2O$		0.612
ZnO	$NaBH_4$ (one-step)	Citric acid	$FeCl_2$		0.559
			$FeSO_4 \cdot 7H_2O$		0.525
			$Fe(acac)_3$		0.629
	H_2	-	$FeSO_4 \cdot 7H_2O$		0.546
			$FeCl_2$		0.595
SiO_2	$NaBH_4$ (one-step)	Citric acid			0.528
MgO					0.546
			$FeSO_4 \cdot 7H_2O$		0.597
			$Fe(acac)_3$		0.589
	H_2	-	$FeSO_4 \cdot 7H_2O$		0.765
			$FeCl_2$		0.796
Charcoal	$NaBH_4$ (one-step)	PVP			0.625
			$FeSO_4 \cdot 7H_2O$		0.542
	H_2	-	$FeSO_4 \cdot 7H_2O$	0.5	0.513
			$FeCl_2$		0.564

Table S2. Elemental analysis of different Fe-supported solids prepared in one-pot.

Support	Organic stabilizer	N %	C %	H %	S %
TiO_2	Citric acid	0.000	0.133	0.499	0.000
TiO_2	PVP	0.104	0.836	1.243	0.000
ZrO_2	Citric acid	0.000	0.113	0.058	0.000
ZnO	Citric acid	0.000	0.208	0.025	0.000

Table S3. Amounts of precursor employed for the synthesis of different Fe-supported catalysts using $NaBH_4$ as a reducing agent.

Iron precursor	wt. % Fe	m (mg)	$NaBH_4$ (mg)
$FeSO_4 \cdot 7H_2O$	0.5	50.04	12.00
	1.5	150.12	36.00
$FeCl_2$	0.5	23.16	12.00
	1.5	69.49	36.00
	5	231.60	120.00
	7	463.20	240.00
$Fe(acac)_3$	0.5	65.19	22.35

Table S4. Amounts of precursor employed for the synthesis of different Fe-supported catalysts using H_2 as a reducing agent.

Iron precursor	wt. % Fe	mass (mg)
$FeSO_4 \cdot 7H_2O$	0.5	50.04
	1.5	150.12
$FeCl_2$	0.5	23.16
	1.5	69.48
$Fe(acac)_3$	0.5	65.19